Abstract

Chapter 1

Introduction

1.1 Introduction

Thermal conductivity is one of the important properties in designing a nuclear fuel, since most of the physical phenomenon are thermally governed. In case of high-performance reactors, fuel goes through high fission density at relatively low temperatures. For this reason research reactor fuels are designed for efficient heat rejection. Usually it is composed of assemblies of thin-plates that uses aluminum alloy cladding. The Reduced Enrichment for Research and Test Reactors (RERR) program was initiated in the US in the late 1970s, to develop new fuels. This development of Low-Enriched Uranium (LEU) fuels for high-performence reactors is an important nonproliferatio initiatives [30]. One of the major requirements is having higher Uranium density to offset the decrease in enrichment. Different alloys have been selected and tested. The U-Mo alloy has been identified as a high performence fuel due to its hgih Uranium density and low neutron capture cross-section [9, 28, 25, 16]. During test operations, it was observed that thermal conductivity decreases with increased burnup. For a fission density of 3.30×10^{21} fissions cm^{-3}, at 200^0C thermal conductivity decreases about 30%, for 4.53×10^{21} fissions cm^{-3} it becomes 45% [4]. Fission also creates a variety of fission products. These fission products consists of gas bubbles, oxide precipitates, metallic precipitates and solid solution in the fuel matrix [26]. Radiation damage and fission products in reactor environment results in complex microstructure evolution which restructures the nuclear fuel over the period of time. Microsturctural evolution

depends on the radial direction of the fuel [31, 23, 20]. For every four fission events one inert gas atom (Xe or Kr) is produced. Xe atoms in U-Mo alloy fuel have a strong tendency to precipitate into small bubble due to their low solubility. The formation and growth of gas bubbles inside irradiated nulcear fuels has techniqual importance since it influences the microstructur of the fuel material [15]. Recent TEM and SEM images show that fission bubble in U-10Mo distribute itself in intergranular and intragranular format. High fission density microstructure shows randomly distributed micron sized fission-gas bubbles distributed throughout the grain boundary. Intergranular bubble density increases with the increase in burnup. Inside the grain fission gas form superlattices. Superlattices have been seen before in the ion irradiated matrial. Typical bubble sizes and spacing in these bubbles are in the range of 2-6.4 nm and 4-12 nm respectively. Usually superlattice has the same crystal structure as the host material, with some exception in some materials. Superlattice in U-10Mo shows a FCC structure in BCC matrix. Ion irradiated bubble superlattice has superlattice constant of 10's of nanometer.

Inclusions and porosity change the thermal and the electrical conductivity of many material. Various models both empirical and analytical, have been proposed to describe this influence. Maxwell [19], was the first one to derive an expression for effective thermal conductivity with an assumption of idealized distribution of spherical particles in a matrix. Few other empirical formulas [18, 11, 8] also exist. The large diversity of shape, porosity and inclusion inside the materials make it impossible to come with one singular equation. Several analytical models describe the influence of porosity and inclusions on the thermal conductivity [19, 17, 7, 35, 3]. These theoritical models are usually valid for pore with regular shape, and the pore arrangment is sufficiently dilute. Numerical methods have also been developed to approximate the effect of porosity and heterogenous microstructure on thermal conductivity. Bakker et. al [2, 1] reconstructed irregular shaped bubble from micrograph of irradiated fuel and meshed for Finite Element Analysis (FEM). Yun et. al [37] performed heat transfer simulation in metallic U-10Zr

fuel with distributed spherical pores. Teague et. al. [32] studied porosity and precipitates in irradited-mixed oxide fuels using 3D microstructure. Recently Hu et al. [14] studied the impact of distributed gas bubble on the effective thermal conductivity of U-Mo metallic fuels using phase field modelling. Microstructure of irradiated nuclear fuels are very complicated. Gas bubbles in irradiated nuclear fuels distribute itself in intra and inter granular way. The size difference between intra and intergranular bubble is very large. The shape is also highly dissimmilar. The intragranular gas bubbles have spherical shape, while intergranular gas have no regular shape. In this work, effective thermal conductivity both inter and intragranular gas bubble

Chapter 2

Methodology

In this work, a Finite Element model is used to solve the steady state heat conduction equation to determinte the effective thermal conductivity of various fuel microstructures. Two types of microstructures were used as simulation domain. Both of the domains contain Xe bubble as fission product. One microstructure (Figure 2.1) contains the Xenon Bubble superlattice sturcture and another microscturcture contains the grain boundary structure (Figure 2.3). The first one represents the intragranular bubble and the second one represents the intergranular bubble. All simulations were performed in 2-D domain. The gas bubble supperlattice structure(GBS) was created based on Miller et al. [21]. According to Miller et al. the bubble size inside the GBS structure follows normal distribution. From these experimental values four diamters were chosen to create FEM model. Since, the GBS inside U-10Mo is FCC, the 2D sturcture was created based on the FCC sturcture. The lattice constant was 12 nm which was also from Miller et al. Lattice constants were kept constants for all four bubble sizes. The bubble sizes were 3.1, 3.6, 3.75 and 4 nm in diameter. The square domains dimension is 80×80 nm, with 91 bubbles inside it with lattice constants of 12. Two dimensional triangulare mesh was used to mesh the domain. Trelis Pro package was used to do the meshing. In the second microsturcture, grain boundary (GB) sturcture is created with Adobe illustrator. The size of the GB structure kept unchanged throughout the drawing. The GB sturcture of U-10Mo was chosen from Miller et al. [22]. This was a SEM (Scanning Electron Microscop image of

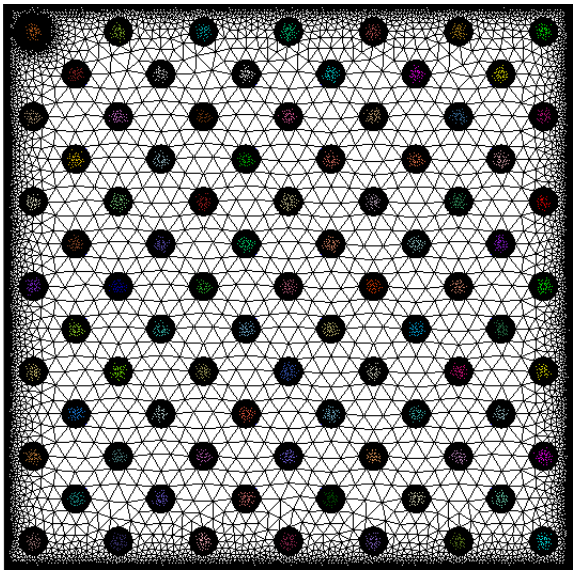

Figure 2.1: Meshed Xenon bubble inside U-10Mo matrix

a FIB (Focused Ion Beam) cross-section showing fission gas bubbles populating in the grain boundaries. This domain was also meshed with triangular mesh. A mesh study was done to chose a meshing size that will optimize the result and the compuational time. The effective thermal conductivity of the domain is determined by applying boundary conditions on each side and solving for temperature field within the domain. In the current work MOOSE Framework [10] was used to obtain the thermal solution.

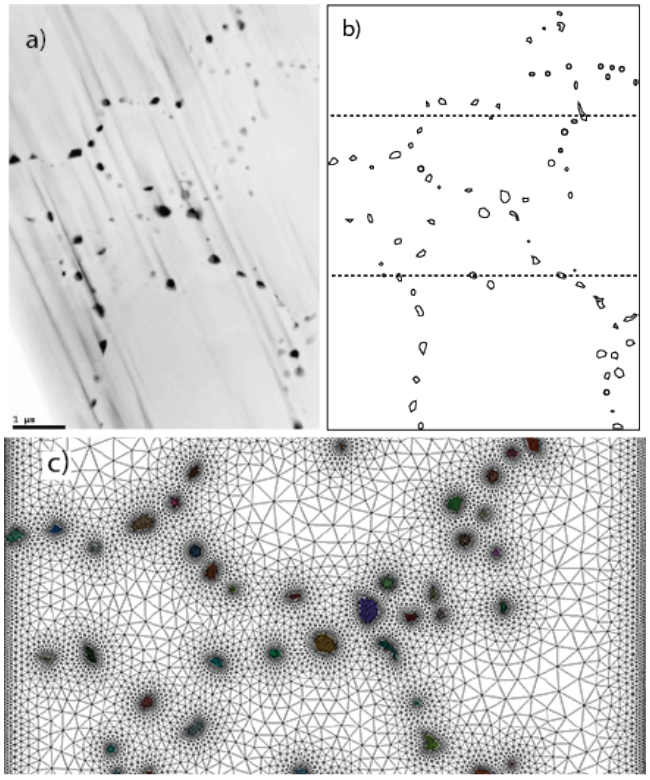

Figure 2.2: a) TEM image of the fission gas bubbles along the grain boundaries from Miller et. al. used for FEM calculations [22] b) Geometry created based on the Grain Boundary fission gas modelling c)FEM mesh with grain boundary fissoin gas

Two material objects were created. Both of these contained the thermal conductivity data for U-10Mo and Xenon. A linear fit of thermal conductivity with respect to temperature was used for U-10Mo which is from Burkes et. al. [5]. Thermal conductivity of Xenon depends both on temperature and pressure [24]. Figure 2.3 shows the change of thermal conductivity with increasing pressure and temperature. Pressure inside the bubble highly depends on the radius and shear modulus of the host material [12, 34]. Xiao et. at. [36] performed atomistic simulation of the small Xenon bubble inside U-MO alloy. According to Xiau et. al. pressure inside the Xenon bubble can go as high as 12 GPa. This increased pressure creates another possibility of having solid Xenon bubbles inside the material [33, 27, 38]. Thermal conductivity data of Xenon above 1000 bar is not available for a wide temeprature range. To evaluate the impact of pressure of Xenon on the overall thermal conductivity, five sets of thermal conductivity data (1bar, 70bar,

220bar, 380bar, 600bar and 1000bar) were used. For each set of data a polynomial fit is used for FEM calculation. The results are discussed in the following section.

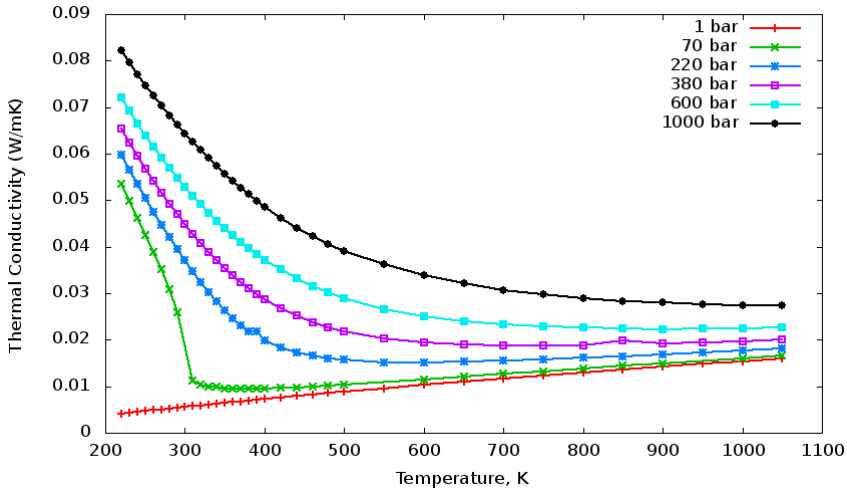

Figure 2.3: Thermal Conductivity of Xenon with increasing pressure from Rabinovich et. al. [24]

Chapter 3

Results

3.1 Results

Figure 3.1 shows the effective thermal conductivity due to Xenon bubble distribution in the intragranular region. Thermal conductivity decreases with the increase in the bubble size. In this simulation thermal conductivity of Xenon was at 1 bar. The FEM result is compared with the theoritical solution for porour material's thermal conductivity, to check whether the FEM results fall in the region. To compare the results the famous Maxwell-Eucken [19] equation was used.

$$\lambda = \lambda_s \frac{\lambda_p + 2\lambda_s + 2\nu_p(\lambda_p - \lambda_s)}{\lambda_p + 2\lambda_s - \nu_p(\lambda_p - \lambda_s)} \tag{3.1}$$

Where, λ = thermal conductivity of the fuel meat

λ_s = thermal conductivity of the continuous phase (U-10Mo)

λ_p = thermal conductivity of the dispersed phase in spherical shape (Xe bubble)

ν_p = volume fraction of the dispersed phase (volume fraction of Xe inside U-10Mo)

Equation 3.1 assumes the pore volume fraction is less than 15% and dispersed uniformely in the solid matrix. The distance between the pores is far enough that they do not interact [6, 29]. The result is also compared with Hashin-Shtrikman upper bound, which is based on a theoritical expression derived for the magnetic permeability of multiphase material [13].

$$\lambda = \frac{1}{4}\left[\lambda_p(3\nu_p - 1) + \lambda_s(2 - 3\nu_p) + \left\{[\lambda_p(3\nu_p - 1) + \lambda_s(2 - 3\nu_p]^2 + 8\lambda_s\lambda_p\right\}^{\frac{1}{2}}\right] \tag{3.2}$$

The compared result is shown in Figure 3.2. As it can be seen from Figure 3.2 that with the increase in temperature there is a slight deviation.

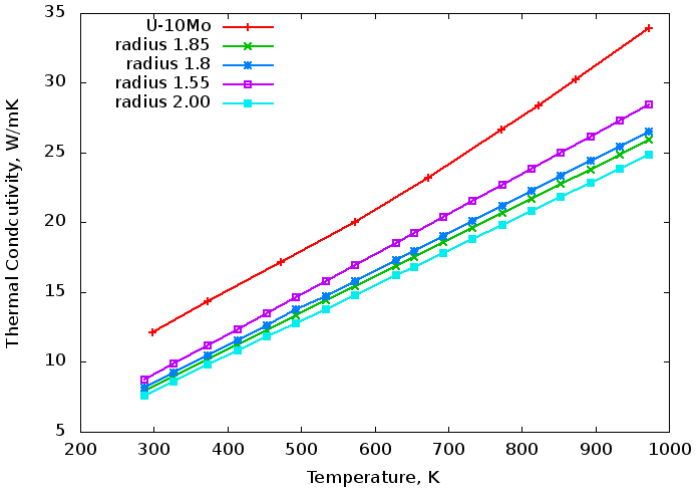

Figure 3.1: Comparison between the thermal conductivity of U-10Mo and the inclusion of Xe bubble of different sizes

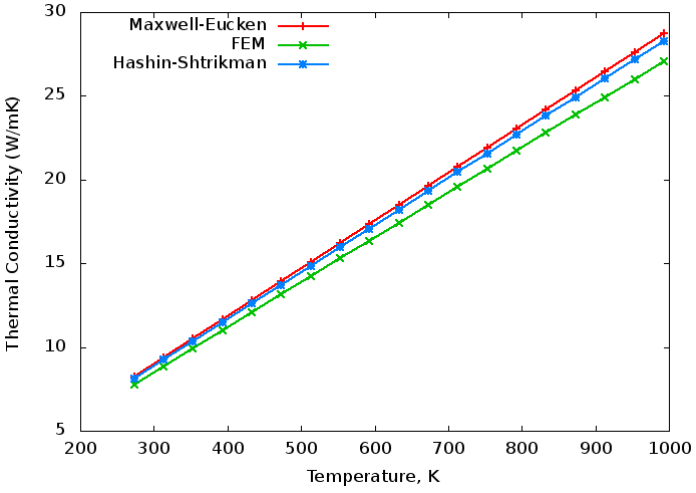

Figure 3.2: Comparison of predicted thermal conductivity of U-10Mo with Xenon bubble against the Maxwell-Eucken and Hashin and Shtrikman

To see tha impact of pressure of Xenon on the overall thermal conductivity, five different pressures were used. Each pressure has a distinctvie thermal conductivity

of Xenon(Figure 2.3). In this study a constant bubble size is used. The result of the simulations is presented in Figure 3.3. The result shows a little to no change on the overall thermal conductivity of the fuel meat. This might be due to the increasing pattern of thermal conductivity with respect to pressure.

To study the grain boundary Xenon bubble, Xenon's thermal conductivity of 1 bar is used. The solution is obtained using Dirichlet boundary condition. The solution is presented in Figure 3.4. With addition of the grain boundary Xenon, overall thermal conductivity drops more than the addition of inragranular bubble.

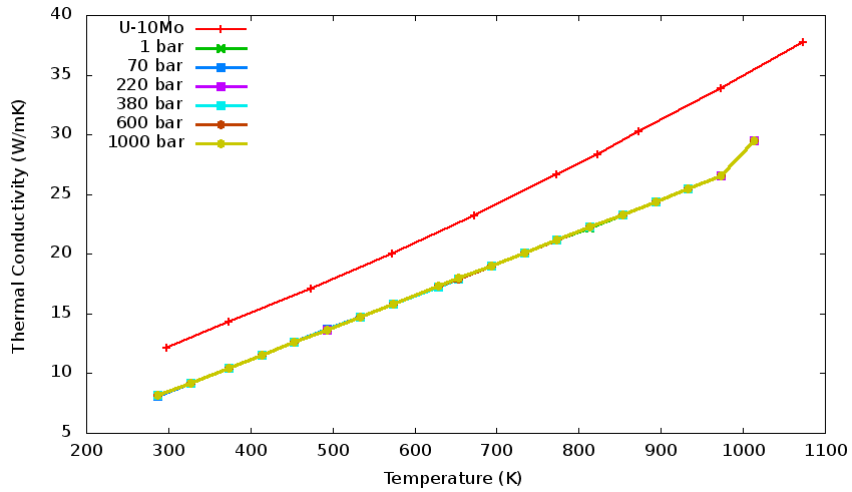

Figure 3.3: Over all thermal conductivity U-10Mo using thermal conductivity of Xenon of several pressure

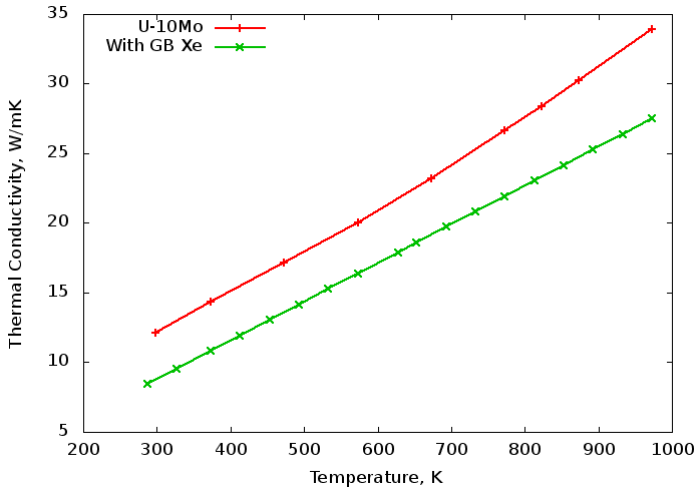

Figure 3.4: Over all thermal conductivity U-10Mo using grain boundary Xenon gas

Chapter 4

Discussions and conclusions

Chapter 5

Acknowledgments

Bibliography

[1] K Bakker. "Using the finite element method to compute the influence of complex porosity and inclusion structures on the thermal and electrical conductivity". In: *International Journal of Heat and Mass Transfer* 40.15 (1997), pp. 3503–3511.

[2] K Bakker, H Kwast, and EHP Cordfunke. "Determination of a porosity correction factor for the thermal conductivity of irradiated U02 fuel by means of the finite element method". In: *Journal of nuclear materials* 226.1-2 (1995), pp. 128–143.

[3] TH Bauer. "A general analytical approach toward the thermal conductivity of porous media". In: *International journal of heat and mass transfer* 36.17 (1993), pp. 4181–4191.

[4] Douglas E Burkes et al. "Thermal properties of U–Mo alloys irradiated to moderate burnup and power". In: *Journal of Nuclear Materials* 464 (2015), pp. 331–341.

[5] Douglas E Burkes et al. "Thermo-physical properties of DU–10wt.% Mo alloys". In: *Journal of Nuclear Materials* 403.1 (2010), pp. 160–166.

[6] CR Clark et al. "Monolithic fuel plate development at Argonne National Laboratory". In: *2003 International Meeting on Reduced Enrichment for Research and Test Reactors, Chicago, IL*. Vol. 1. 10. 2003.

[7] ME Cunningham and KL Peddicord. "Heat conduction in spheres packed in an infinite regular cubical array". In: *International Journal of Heat and Mass Transfer* 24.7 (1981), pp. 1081–1088.

[8] MF DeVries. "An experimental determination of the thermal conductivity of a 304L stainless steel powder metallurgy material". In: *Journal of Heat Transfer* 111 (1989), p. 281.

[9] A Ewh et al. "Microstructural Characterization of U-Nb-Zr, U-Mo-Nb, and U-Mo-Ti Alloys via Electron Microscopy". In: *Journal of phase equilibria and diffusion* 31.3 (2010), pp. 216–222.

[10] Derek Gaston et al. "MOOSE: A parallel computational framework for coupled systems of nonlinear equations". In: *Nuclear Engineering and Design* 239.10 (2009), pp. 1768–1778.

[11] LA Goldsmith and JAM Douglas. "Measurements of the thermal conductivity of uranium dioxide at 670–1270 K". In: *Journal of Nuclear Materials* 47.1 (1973), pp. 31–42.

[12] GW Greenwood, AJE Foreman, and DE Rimmer. "The role of vacancies and dislocations in the nucleation and growth of gas bubbles in irradiated fissile material". In: *Journal of Nuclear Materials* 1.4 (1959), pp. 305–324.

[13] Zvi Hashin and Shmuel Shtrikman. "A variational approach to the theory of the effective magnetic permeability of multiphase materials". In: *Journal of applied Physics* 33.10 (1962), pp. 3125–3131.

[14] Shenyang Hu et al. "Assessment of effective thermal conductivity in U–Mo metallic fuels with distributed gas bubbles". In: *Journal of Nuclear Materials* 462 (2015), pp. 64–76.

[15] Yeon Soo Kim and GL Hofman. "Fission product induced swelling of U–Mo alloy fuel". In: *Journal of Nuclear Materials* 419.1 (2011), pp. 291–301.

[16] A Landa, P Söderlind, and PEA Turchi. "Density-functional study of bcc U–Mo, Np–Mo, Pu–Mo, and Am–Mo alloys". In: *Journal of Nuclear Materials* 434.1 (2013), pp. 31–37.

[17] Arthur L Loeb. "Thermal conductivity: VIII, a theory of thermal conductivity of porous materials". In: *Journal of the American Ceramic Society* 37.2 (1954), pp. 96–99.

[18] JB MacEwan, RL Stoute, and MJF Notley. "Effect of porosity on the thermal conductivity of UO2". In: *Journal of Nuclear Materials* 24.1 (1967), pp. 109–112.

[19] James Clerk Maxwell. *A treatise on electricity and magnetism*. Vol. 1. Clarendon press, 1904, p. 440.

[20] MK Meyer et al. "Irradiation performance of U-Mo monolithic fuel". In: *Nuclear Engineering and Technology* 46.2 (2014), pp. 169–182.

[21] BD Miller et al. "Transmission electron microscopy characterization of the fission gas bubble superlattice in irradiated U–7wt% Mo dispersion fuels". In: *Journal of Nuclear Materials* 458 (2015), pp. 115–121.

[22] Brandon D Miller et al. "Advantages and disadvantages of using a focused ion beam to prepare TEM samples from irradiated U–10Mo monolithic nuclear fuel". In: *Journal of Nuclear Materials* 424.1 (2012), pp. 38–42.

[23] J Noirot, L Desgranges, and J Lamontagne. "Detailed characterisations of high burn-up structures in oxide fuels". In: *Journal of Nuclear Materials* 372.2 (2008), pp. 318–339.

[24] Viktor Abramovich Rabinovich et al. "Thermophysical properties of neon, argon, krypton, and xenon". In: (1987).

[25] J Rest, GL Hofman, and Yeon Soo Kim. "Analysis of intergranular fission-gas bubble-size distributions in irradiated uranium–molybdenum alloy fuel". In: *Journal of Nuclear Materials* 385.3 (2009), pp. 563–571.

[26] Vincenzo V Rondinella and Thierry Wiss. "The high burn-up structure in nuclear fuel". In: *Materials today* 13.12 (2010), pp. 24–32.

[27] M Ross and AK McMahan. "Condensed xenon at high pressure". In: *Physical Review B* 21.4 (1980), p. 1658.

[28] DE Smirnova et al. “A ternary EAM interatomic potential for U–Mo alloys with xenon”. In: *Modelling and Simulation in Materials Science and Engineering* 21.3 (2013), p. 035011.

[29] David S Smith et al. “Thermal conductivity of porous materials”. In: *Journal of Materials Research* 28.17 (2013), pp. 2260–2272.

[30] James L Snelgrove et al. “Development of very-high-density low-enriched-uranium fuels”. In: *Nuclear Engineering and Design* 178.1 (1997), pp. 119–126.

[31] H Stehle. “Performance of oxide nuclear fuel in water-cooled power reactors”. In: *Journal of Nuclear Materials* 153 (1988), pp. 3–15.

[32] Melissa C Teague et al. “Using coupled mesoscale experiments and simulations to investigate high burn-up oxide fuel thermal conductivity”. In: *Jom* 66.12 (2014), pp. 2569–2577.

[33] LE Thomas. “Condensed-phase xenon and krypton in UO2 spent fuel”. In: *Fundamental aspects of inert gases in solids*. Springer, 1991, pp. 431–441.

[34] H Trinkaus. “Energetics and formation kinetics of helium bubbles in metals”. In: *Radiation Effects* 78.1-4 (1983), pp. 189–211.

[35] Da Yu Tzou. “The effect of internal heat transfer in cavities on the overall thermal conductivity”. In: *International journal of heat and mass transfer* 34.7 (1991), pp. 1839–1846.

[36] Hongxing Xiao et al. “Atomistic simulations of the small xenon bubble behavior in U–Mo alloy”. In: *Materials & Design* 74 (2015), pp. 55–60.

[37] Di Yun et al. “Simulation of the impact of 3-D porosity distribution in metallic U–10Zr fuels”. In: *Journal of Nuclear Materials* 448.1 (2014), pp. 129–138.

[38] J Zheng et al. “Thermodynamics, compressibility, and phase diagram: Shock compression of supercritical fluid xenon”. In: *The Journal of chemical physics* 141.12 (2014), p. 124.

Appendix A

XYZ Algorithm

```
clc
clear all
NN=input('Input the value of N');
%------next 13 lines assign an index IG to each basis function
C=zeros(3,3,3,3);
IG=0;
for I=1:3
    for L=1:NN+1
        for M=1:NN+1
            for N=1:NN+1
             if (L+M+N > NN+3), break, end
             IG=IG+1;
             IC(IG)=1;
             LB(IG)=1;
             MB(IG)=1;
             NB(IG)=1;

            end
        end
    end

end
rank=0.5*(NN+1)*(NN+2)*(NN+3);
NR=IG;
Gamma=zeros(rank,rank);
for IG=1:NR
     for JG=IG:NR
         I=IC(IG);
         J=IC(JG);
         LS=LB(IG)+LB(JG);
         MS=MB(IG)+MB(JG);
         NS=NB(IG)+NB(JG);

         Gamma(IG,JG)=C(I,1,J,1)*LB(IG)*LB(JG)*func(LS-2,MS,NS)+...
```

```
            C(I,2,J,2)*MB(IG)*MB(JG)*func(LS,MS-2,NS)+...
            C(I,3,J,3)*NB(IG)*NB(JG)*func(LS,MS,NS-2)+...
            C(I,1,J,2)*LB(IG)*MB(JG)+...
            C(I,2,J,1)*MB(IG)*LB(JG)*func(LS-1,MS-1,NS)+...
            C(I,1,J,3)*LB(IG)*NB(JG)+...
            C(I,3,J,1)*NB(IG)*LB(IG)*func(LS-1,MS,NS-1)+...
            C(I,2,J,3)*MB(JG)*NB(IG)+...
            C(I,3,J,2)*NB(IG)*MB(JG)*func(LS,MS-1,NS-1);
    Gamma(JG,IG)=Gamma(IG,JG);
  if(I==J) E(IG,IG)=func(LS,MS,NS) ;
    end
end
end


[vects vals]=eig(E\Gamma);
```